

Stealing Maggie’s Secrets—On the Challenges of IP Theft Through FPGA Reverse Engineering

Simon Klix
MPI-SP
Bochum, Germany

Nils Albartus
MPI-SP
Bochum, Germany

Julian Speith
MPI-SP
Bochum, Germany

Paul Staat
MPI-SP
Bochum, Germany

Jörn Langheinrich
MPI-SP
Bochum, Germany

Alice Verstege
Ruhr University Bochum
Bochum, Germany

Annika Wilde
Ruhr University Bochum
Bochum, Germany

Daniel Lammers
Ruhr University Bochum
Bochum, Germany

Christian Kison
Bundeskriminalamt
Wiesbaden, Germany

Sebastian Sester-Wehle
Bundeskriminalamt
Wiesbaden, Germany

Daniel Holcomb
UMass Amherst
Amherst, MA, USA

Christof Paar
MPI-SP
Bochum, Germany

ABSTRACT

Intellectual Property (IP) theft is a cause of major financial and reputational damage, reportedly in the range of hundreds of billions of dollars annually in the U.S. alone. Field Programmable Gate Arrays (FPGAs) are particularly exposed to IP theft, because their configuration file contains the IP in a proprietary format that can be mapped to a gate-level netlist with moderate effort. Despite this threat, the scientific understanding of this issue lacks behind reality, thereby preventing an in-depth assessment of IP theft from FPGAs in academia. We address this discrepancy through a real-world case study on a Lattice iCE40 FPGA found inside iPhone 7. Apple refers to this FPGA as *Maggie*. By reverse engineering the proprietary signal-processing algorithm implemented on Maggie, we generate novel insights into the actual efforts required to commit FPGA IP theft and the challenges an attacker faces on the way. Informed by our case study, we then introduce generalized netlist reverse engineering techniques that drastically reduce the required manual effort and are applicable across a diverse spectrum of FPGA implementations and architectures. We evaluate these techniques on six benchmarks that are representative of different FPGA applications and have been synthesized for Xilinx and Lattice FPGAs, as well as in an end-to-end white-box case study. Finally, we provide a comprehensive open-source tool suite of netlist reverse engineering techniques to foster future research, enable the community to perform realistic threat assessments, and facilitate the evaluation of novel countermeasures.

CCS CONCEPTS

• Security and privacy → Hardware reverse engineering.

KEYWORDS

FPGA reverse engineering, IP theft, bitstream, gate-level netlist

1 INTRODUCTION

Many companies invest heavily into creating intellectual property (IP), which often forms the backbone of their economic value and competitive advantage. For instance, Apple alone spent over \$26 billion on research and development (R&D) in 2022 [32]. Not surprisingly, valuable IP can nowadays often be found within electronics and integrated circuits (ICs) in particular. It can take the

form of proprietary algorithms for domains like digital signal processing (DSP), CPUs, or security functions. As a flip side of this development, IP theft, e.g., by competitors or hostile nation states, has become a major issue. In the U.S. alone, IP theft causes hundreds of billions of dollars in damages every year, with the semiconductor market being of particular concern [35]. In this paper, we look at an important aspect of this issue, namely assessing the security of IP in field-programmable gate arrays (FPGAs), which are, as we argue, particularly vulnerable against IP theft.

In many highly specialized domains—such as spaceflight, military communications, network routers, or medical devices—FPGAs are a vital component, often incorporating proprietary IP. FPGAs are (re-)configurable logic devices that are programmed using a bitstream with a proprietary file format. This bitstream is generated by electronic design automation (EDA) tools provided by the FPGA vendors. These tools map a high-level design, written in a hardware description language (HDL) such as Verilog, to a bitstream during synthesis. At the end of this process, the implemented IP is fully encapsulated in the bitstream file. This file is stored externally to the FPGA but resides on the target device.

Improving our understanding of the associated challenges and required efforts is crucial to better assess the threat of, and defend against, real-world IP theft from FPGA implementations. In most cases, hardware IP theft entails reverse engineering the design in order to recover the implemented algorithms and their instantiation.

Modern nanometer-scale ICs come with a natural defense against reverse engineering due to the high cost and labor-intensive nature of the netlist extraction process [22, 38, 56, 70, 71]—a financial barrier that deters all but the most resourceful entities, such as nation-states. However, the bar for FPGA reverse engineering is much lower. To this end, an attacker would need to access the bitstream and map it to a gate-level netlist. This process is already well understood despite the proprietary nature of the bitstream format [4, 10, 15, 20, 51, 52, 55, 76]. FPGA vendors commonly provide cryptographic bitstream protections as a safeguard for valuable IP. Nonetheless, these measures have repeatedly been demonstrated to be susceptible to side-channel attacks [46–48, 67, 68] or protocol flaws [18, 19]. Many low-cost FPGAs do not even offer such protections. Even if these protective measures are available and resist such attacks, they must be *proactively* enabled by the FPGA

developer. Hence, we assume access to the plaintext bitstream, and thus the gate-level netlist, is generally achievable in practice.

In this situation, a reverse engineer is typically faced with a gate-level netlist that lacks any hierarchy, module boundaries, and word-level information such as data types, see Section 2.3. Many netlist reverse engineering techniques have tried to address these challenges in recent years [7], but they often deal only with isolated sub-problems such as register recovery, lack reference implementations, and use unrealistic and/or outdated benchmarks, see Section 5.3. In particular, an end-to-end analysis of a real-world FPGA design remains largely unexplored in literature. As a consequence, the actual threat potential of FPGA IP theft as well as the unique challenges it entails remain unknown. Thus, the motivation of the paper at hand is to investigate the reverse engineering of a complex FPGA netlist that is recovered from a real-world device in a black-box setting. The goal is to obtain and analyze the algorithmic description of the design. A better understanding of this issue can aid in the design of sound defenses and inform risk analysis of industry as well as governments. FPGA reverse engineering also paves the way for attacks other than IP theft, e.g., retrieving hard-coded cryptographic keys or inserting hardware Trojans.

Research Questions and Contributions. For a realistic assessment of real-world FPGA reverse engineering challenges in the context of IP theft, we first set out to answer the following research question:

RQ1: What challenges and efforts are entailed with IP theft through FPGA reverse engineering in a black-box setting?

To answer RQ1, we demonstrate the steps and efforts required to extract IP from an FPGA implementation through a case study on a Lattice iCE40 FPGA found within the iPhone 7. Apple refers to this FPGA as *Maggie* in the iPhone firmware. To this end, we combine existing techniques and propose new approaches to recover an algorithmic description of the target FPGA implementation, effectively extracting the IP controlling the iPhone’s *Taptic Engine*, see Section 3. In addition to evaluating existing techniques and proposing novel approaches to FPGA reverse engineering, we provide unique insights that foster developing better defenses against IP theft. Based on our findings, a second research question arises:

RQ2: To what extent can FPGA reverse engineering be generalized across architectures and implementations?

In response to RQ2, we generalize the methods developed for our case study. This yields automated methods that are applicable across FPGA architectures and implementations. In particular, we target Xilinx 7-Series and Lattice iCE40 FPGA families, see Section 4. We evaluate the presented techniques in isolation on a diverse set of benchmark netlists and discuss differences in effectiveness. Additionally, we conduct an end-to-end white-box case study to demonstrate the effectiveness of our workflow as a whole. In line with the efforts of the security community to provide open-source implementations, thereby removing financial barriers and enabling third-party verification, we share our benchmarks and implementations as plugins to HAL [29]. Thereby, we hope to encourage more insight into FPGA reverse engineering in follow-up work by academia and industry, and foster the development of countermeasures, see Section 5.

Responsible Disclosure. Despite not revealing any security vulnerabilities, we informed Apple and Lattice Semiconductor about our findings before publication. In agreement with the vendors, we will not publish the gate-level netlist recovered from Maggie’s bitstream or our bitstream conversion tooling for Lattice iCE40 FPGAs.

2 ATTACKER MODEL & CHALLENGES

2.1 Attacker Model

Our attacker model revolves around IP theft, which is a common threat considered in hardware security research [21, 60]. An attacker obtains a device featuring an FPGA and aims to recover the contained IP by extracting an algorithmic model of the design implemented on the FPGA by means of reverse engineering. We assume the attacker has gained access to the bitstream configuring the FPGA by either extracting it from the device or from firmware. Given that the attacker possesses the device, they can execute the FPGA implementation and modify the hardware as needed.

As is typical in reverse engineering, the attacker may have already gathered public information on the target device, such as documentation or patents. This leaves them with knowledge on the system’s connectivity and interaction with the FPGA, along with a general understanding of its purpose, but lacking detailed knowledge of the implementation and the intricacies of the algorithm. Ultimately, the attacker seeks to reconstruct a detailed algorithmic representation that allows him to extract, understand, and modify the IP contained within it. Thus, our attacker model explicitly goes beyond simply copying an FPGA bitstream or netlist.

2.2 Netlist Reverse Engineering Terminology

A gate-level netlist is a digital circuit representation comprising combinational and sequential *gates* or standard cells as well as their interconnections, also known as *nets*. In reverse engineering, we frequently encounter flattened netlists lacking hierarchy or module boundaries. Furthermore, we differentiate between *data path* and *control path*. The control path steers the data path in that it decides which operations are being performed on the data passing through by enabling or disabling certain parts of the circuit.

Reverse engineering gate-level netlists involves *static* and *dynamic* techniques. Static methods analyze the netlist graph and can take either *structural* or *functional* information into account. Dynamic techniques leverage data gathered during execution to reverse engineer functionality.

2.3 Challenges of Netlist Reverse Engineering

Committing IP theft on an FPGA requires analyzing the gate-level netlist extracted from the bitstream, posing unique challenges. These challenges arise from the need to reconstruct information removed during synthesis. The challenges we faced include:

- C1: Loss of Hierarchy.** HDL designs feature modules that encapsulate functionality and introduce hierarchy. This information is removed during synthesis. The resulting netlist lacks any module boundaries or hierarchy.
- C2: Loss of Data Types.** An HDL description makes use of multi-bit data types like integers on which, e.g., arithmetic operations are performed. In contrast, gate-level netlists only contain gates

and nets operating on bit level. Not only is the information of which gates belong to the same word-level operation lost during synthesis, but also the order of bits within word-level structures. Consequently, high-level data types no longer exist in the netlist which hampers analysis relying on, e.g., integer values.

C3: Synthesizer Optimizations. Synthesizer optimizations can result in similar operations on HDL level looking vastly different in a gate-level netlist. Logic may be merged across module boundaries and gates or even entire sub-circuits may be duplicated to facilitate a high fan-out. Such optimizations always depend on the available standard cells, timing and area constraints, routing requirements, and varying optimization strategies.

C4: Missing Control Separation. The control path is often implemented using finite state machines (FSMs). In an HDL design, FSMs can be distinguished from one another and the data path. In netlists, FSMs are often merged with one another or even the data path such that boundaries can no longer be determined. This causes a state explosion when analyzing affected FSM state graphs, sometimes raising complexity beyond what is feasible.

C5: Data Dependency. In our case study, the behavior of the control path—and in extension the data path—depended on external data and instructions fed to the FPGA as input. Hence, analyzing such a netlist without input data is challenging, especially if the control path cannot be properly dissected.

C6: Dynamic Behavior. Sequential gates add another dimension to netlist reverse engineering in that they require the reverse engineer to consider past states for the analysis of current behavior. This blows up complexity due to the vast number of possible netlist states to consider.

C7: Semantic Analysis. Extracting a word-level algorithmic representation leaves a reverse engineer with the task of assigning meaning and symbols to different values of the computation. To gain a high-level understanding, including the underlying rationale and specific design decisions, the functionality needs to be dissected rigorously from the system level down to individual building blocks, calling for domain-specific expertise.

3 CASE STUDY ON IPHONE 7

To answer RQ1 and investigate the effort required to commit IP theft from a real-world FPGA implementation, we conducted a case study on an FPGA found in iPhone 7.

Target Device. The iPhone 7 and iPhone 7 Plus were released in September 2016. The smartphones feature a novel capacitive home button with haptic feedback being generated by the *Taptic Engine* first introduced in Apple Watch and iPhone 6s. Notably, both iPhone 7 and iPhone 7 Plus contain a Lattice iCE5LP4K-SWG36 FPGA. Apple refers to this chip as *Maggie* throughout firmware and leaked printed circuit board (PCB) schematics. There are many speculations revolving around the purpose of Maggie [31, 40, 69].

Setting. From analyzing leaked PCB schematics, the iPhone firmware, and patents granted to Apple [27, 28], we concluded that Maggie controls the *Taptic Engine*, and determined its I/O connectivity and communication interfaces, see Figure 1. This alone does not enable effective IP theft, as we still lack implementation details on the

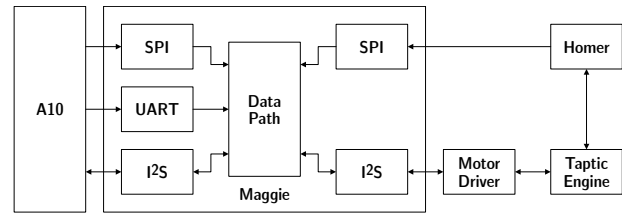


Figure 1: Maggie as part of the Taptic Engine controller.

instantiated signal processing algorithms and their parameters. Assuming the role of the attacker, we therefore need to investigate the circuit implemented on Maggie to fully recover Apple's Taptic Engine IP. To this end, we split the iPhone FPGA reverse engineering process into four steps, see Figure 2.

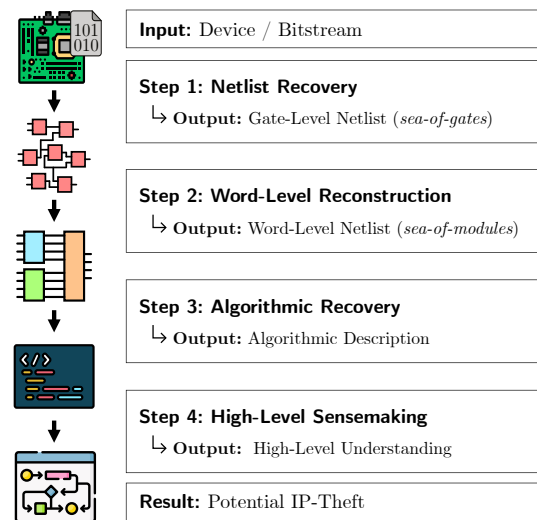


Figure 2: Overview of our case study on iPhone 7.

3.1 Step 1: Netlist Recovery

At first, we were faced with the iPhone 7 containing the bitstream featuring the target IP and our first goal was to extract the gate-level netlist for further analysis.

Bitstream Acquisition. SRAM-based FPGAs such as Lattice iCE40 devices store the bitstream externally and are configured during startup. Hence, an attacker can read the bitstream from external memory, intercept it during transmission, or recover it from device firmware. The Maggie bitstream is shipped with the openly available iPhone firmware, hence we extracted it from the file system. The original bitstream was published in September 2016 and was updated with iOS 10.2 in December 2016. As it remains unchanged ever since, our analysis deals with this latest version.

Bitstream Format Reverse Engineering. The bitstream format is typically a secret well-kept by FPGA vendors, although everyone can generate bitstreams using respective EDA tools. Project Icestorm [3] entails a comprehensive documentation database of the

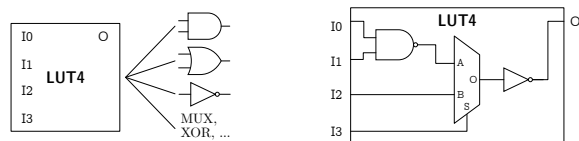
Lattice iCE40 bitstream format generated by fuzzing the Lattice iCEcube2 EDA tool. Project IceStorm is part of F4PGA [2], an open-source EDA tool-flow developed as an alternative to proprietary vendor software. As part of our efforts, we extended Project IceStorm by increasing its fuzzing coverage and adding support for the pinout of Maggie’s SWG36 chip package.

Bitstream Conversion. Given a database detailing the mapping from bits to netlist elements, an arbitrary bitstream can be converted back to a gate-level netlist in full automation. In light of our case study, we developed a custom bitstream conversion tool that translates any Lattice iCE40 bitstream into a gate-level netlist. Our tool depends on the Project IceStorm database to be complete and correct. For Maggie, we observed 36 nets with missing sources or destinations, hinting at an incomplete bitstream database. Later on, we manually repaired these nets using information on surrounding circuitry revealed once our analysis progressed. The extracted netlist contains 5046 gates comprising 3241 look-up tables (LUTs), 422 carry gates, 1342 flip-flops (FFs), 18 block-RAMs (BRAMs), and 4 DSP units.

3.2 Step 2: Word-Level Reconstruction

After extracting the gate-level netlist, we aimed to recover word-level structures from the unstructured sea-of-gates using the netlist reverse engineering framework HAL [29]. To this end, we were confronted with the challenges outlined in Section 2.3.

Netlist Pre-Processing. We initially pre-processed the netlist to eliminate synthesis byproducts hindering analysis and enhance readability for human reverse engineers.



(a) Replace LUTs with primitive combinational gates. (b) Decompose LUTs into a MUX and primitive gates.

Figure 3: Netlist Preparation Overview.

For more efficient manual analysis and considering that some LUTs merely implement basic functions like AND or XOR, we substituted such LUTs with primitive gates, see Figure 3a. We also removed buffer LUTs as they add no functionality but sometimes hinder structural analysis. Furthermore, we removed gates and sub-circuits that compute the same function on identical inputs. The synthesizer introduces such duplicates for optimization purposes, yet they can obfuscate shared control signals or data inputs.

MUXes in particular provide structure to the data path. On FPGAs, however, their functionality is implemented as part of more complex Boolean functions within LUTs. Hence, decomposing complex LUTs into small building blocks such as MUXes can aid manual and automated reverse engineering, e.g., by supporting structural analysis. To recover nested MUXes and better understand the data path (see Figure 5), we analyzed each LUT’s Boolean function and searched for inputs that behave like a select. When discovering a MUX in a LUT, we replaced the LUT with a MUX and reconstruct

the surrounding logic from primitive gates. In total, we replaced 549 LUTs with primitive gates, removed 594 buffers, extracted 1619 MUXes and 1161 primitive gates, removed 353 duplicate gates, and removed 51 additional gates using other simplifications.

Control Logic. Analyzing Maggie’s control path was required for comprehending how the circuit operates. Additionally, certain techniques operating on the data path require knowledge of which gates and nets belong to the control path. Unfortunately, the absence of FPGA-compatible reference implementations [25, 43, 44], the absence of public implementations altogether [11, 12, 23, 61], or general assumptions on strongly connected components (SCCs) that do not always hold for our case study [23, 61], prevented us from applying existing techniques from literature. In particular, the NETA toolset [45] is only available as binaries that cannot parse FPGA netlists. Moreover, a common assumption is that the state registers and transition logic of an FSMs form an SCC [23, 61]. For Maggie, we found 55 SCCs with all but seven comprising three gates or less. Vast parts of the netlist form a single SCC of more than 5000 gates. Therefore, SCCs are not useful in our case study.

Given the intricacies of this issue, we could not find a workable solution within the scope of this work and hence decided to manually investigate the control path of Maggie instead. Here, we faced significant challenges due to the FSMs being interwoven to an extent that often prevented even manual separation, as discussed in [12]. While FSM separation was not always feasible, we still classified FFs as part of the control path by checking whether they feed into control pins such as MUX select or FF enable. After assigning a FF to the control path, we examined its predecessors and successors. These structural characteristics are merely clues that a gate might belong to the control path. They often required manual inspection and human intuition, hence preventing full automation.

Communication Interfaces. Investigating Maggie’s SPI, UART, and I²S interface implementations (see Figure 1) supports word-level structure recovery as these interfaces often comprise the first or last register of a data path. Furthermore, we must reverse engineer these interfaces to understand the parallel and serial conversion of incoming and outgoing data, which is a precondition for recovering bit orders and data types. Through manual reverse engineering, we identified 615 gates belonging to five interfaces.

Arithmetic Structures. In the iPhone netlist, we observed the data path comprising mostly combinational logic implemented as LUTs and carry gates as well as sequential logic implemented using FFs. Some data-path structures are implemented in a consistent, recurring way, e.g., adders, counters, and selected comparators. Lattice iCE40 FPGAs provide carry gates that are commonly connected to form carry chains, often used in combination with LUTs to implement arithmetic operations, see Figure 4. A reverse engineer can leverage these recurring patterns to identify word-level structures like adders or counters in a gate-level netlist.

To recover word-level arithmetic operations, we first located carry chains in the netlist by scanning for connected carry gates. We then assembled arithmetic structure candidates by adding surrounding logic to the carry chains. Since a structure may be influenced by control inputs, we constructed structural candidate

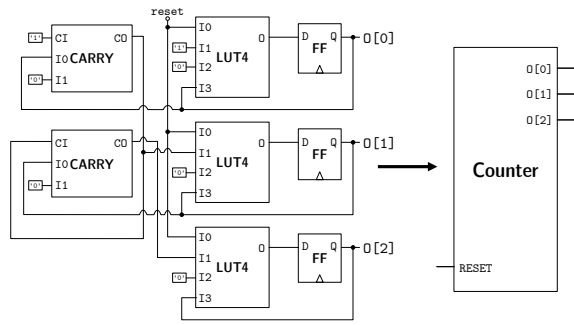


Figure 4: Structure of a 3-bit counter with reset constructed from a carry chain on a Lattice iCE40 FPGA.

variants to account for different control behaviors. Operand membership and the order of input and output signals were derived from the structure and connectivity of a candidate’s gates. For example, the order of inputs was reconstructed by identifying the carry gate of the chain that a signal is connected to. Finally, we checked each candidate against predefined satisfiability modulo theories (SMT) models, e.g., $A \pm B$ for adders or $A \pm n$ for counters incrementing by a constant n .

Sequential Data Path. The synthesizer realizes word-level registers from the HDL design as individual FFs that lack any indication of which register they belong to. To this end, DANA [1] can be used to recover these word-level registers from a gate-level netlist using structural metrics such as shared predecessors and successors as well as common control signals. However, as DANA is optimized for data-path analysis, control FFs may not be recognized as such and instead be wrongfully merged into data-path registers. This impairs the detection of other registers due to DANA’s iterative nature. Hence, we extended DANA to include *known registers* identified by other analysis techniques for finding, e.g., communication interfaces, FSMs states, and counters. DANA does not alter these registers but utilizes them to identify registers further up or down the data path.

Combinational Data Path. In the data path, MUXes can be used to switch between word-level data sources, such as global inputs, memory, or arithmetic structures. We implemented a method to group MUXes that have been decomposed from LUTs as part of our pre-processing, see Figure 3. A MUX selects an input to be forwarded to the output based on a select input S . Multiple MUXes sharing a common select typically form a word-level MUX structure. Detecting such structures allows for the separation of word-level data paths, see Figure 5. However, grouping by select can yield oversized structures as the same select signal may influence two or more distinct data paths. Hence, we split these groups according to preceding or successive word-level structures. For example, if a 32-bit MUX was succeeded by two 16-bit registers, the MUX was split into two 16-bit MUXes. As other preceding or successive MUXes themselves were considered for splitting, the process was repeated iteratively until no further changes could be observed.

Bit Order. While the order of signals (i.e., the *bit order*) belonging to a word is inherently known in the HDL design, it is removed during

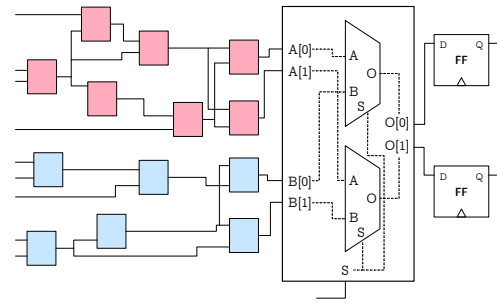


Figure 5: The recovery of word-level MUXes allows for the analysis of separate independent data paths.

synthesis. Hence, for a reverse engineer it is not clear which bits of, e.g., a register are the LSB or MSB. Recovering the bit order of word-level structures aids manual investigation of the design and is vital for the reconstruction of data types used during simulation, see Section 3.3. For adders, counters, BRAMs, and DSPs, the bit order can be inferred from their topology and function. Implementations of other structures, e.g., word-level registers and MUXes, do not exhibit an obvious bit order.

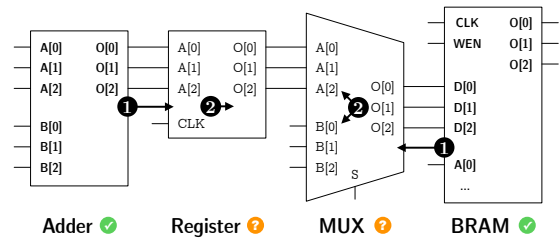


Figure 6: The bit orders of the adder and the BRAM are known, but not those of the register and the MUX. In iteration 1, the order of adder pin group 0 is propagated to register pin group A; the order of BRAM pin group D is propagated to MUX pin group 0. In iteration 2, both orders are propagated within the register and the MUX to cover their outputs and inputs. Finally, the algorithm terminates as all bit orders have been annotated.

We propagated the bit order from structures with known bit order along the data path to structures with unknown bit order. For every unordered pin group, our algorithm (i) derives bit-order candidates from predecessors and successors and (ii) tries to establish consensus between them. Candidates with inherent conflict are discarded, e.g., when different pins of a pin group fetched the same index from the same origin. We omit control logic during analysis, as it does not feature a natural bit order and degrades results.

Outcome. Table 1 depicts the results for our automated techniques. In addition, we manually grouped 688 gates into data-path modules that did not feature MUXes and identified 631 gates belonging to control logic. In total, we assigned 4570 out of 5496 gates (83%) to structures using manual and automated techniques. Furthermore,

we assigned a bit order to 605 (71%) out of 843 pin groups from word-level structures that were not classified as control logic. While we could not verify against a ground truth as of the black-box nature of our case study, these results enabled correctly extracting the implemented algorithm, thereby underlining their value.

Structure	#Recovered	#Gates	Automated?
Arithmetic	35	692	✓
Register	118	1342	✓
Multiplexers	160	1217	✓

Table 1: Results of our word-level reconstruction.

3.3 Step 3: Algorithmic Recovery

Having previously recovered word-level structures, we extracted an algorithmic description of what the iPhone netlist implements. This entails further analyzing the control path, as we could not draw boundaries between individual control structures so far.

Virtual Probing. Instead of further attempting to unravel the semantics of the interwoven control logic, we decided to use dynamic reverse engineering techniques to observe the actual behavior of the circuit at runtime. However, such dynamic analysis often requires expensive equipment and yields only incomplete insights into the execution state [50, 68]. Hence, we leveraged a more workable approach: netlist simulation using I/O signals captured during operation. We further used this approach to (i) observe the flow of real-world data through the netlist, assisting in algorithmic recovery, and (ii) to verify correctness of the recovered netlist and the later extracted algorithm implemented on Maggie by comparing simulation results against recorded outputs.

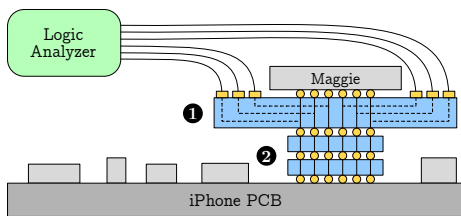


Figure 7: A breakout board is placed between Maggie and the iPhone 7 PCB to record Maggie’s I/O. The breakout board comprises two parts: ① a wider PCB passing the signals to Maggie and to a logic analyzer and ② two small PCB cubes vertically routing the signals

We captured I/O signals by placing a custom breakout board between Maggie and the iPhone PCB, see Figure 7. By feeding the captured I/O signals to a simulator, we could then analyze the state of the circuit at any point in time. This reduced complexity of the circuit’s theoretical state space by focusing only on the states that are actually reached. To this end, we extended the netlist analysis framework HAL [29] with simulation capabilities, see Appendix A. This approach allowed for, e.g., analysis of the data flow over time

and correct traversal of states for complex FSMs that otherwise exhausted functional analysis. Given the previously reconstructed word-level structures and their bit orders, we could now follow the flow of multi-bit data through the design and observe which operations were executed at what point in time. This completely alleviated us from the need to statically analyze the control path.

DSP Analysis. By tracing inputs to Maggie through the netlist in simulation, we found that almost all data-path operations are performed by four connected DSPs. On Lattice iCE40 FPGAs, DSPs feature four 16-bit data inputs and a 32-bit output [58]. On Maggie, all DSPs are configured as Multiply-Accumulate (MAC) units performing 16-bit multiplication and 32-bit accumulation. Most DSP inputs are preceded by LUTs implementing MUXes to allow for dynamically changing data sources, see Figure 8. Each DSP and its MUXes are controlled by an FSM. Looking at the simulation, we found that every DSP computes a recurring sequence of operations depending on dynamically changing control and data inputs.

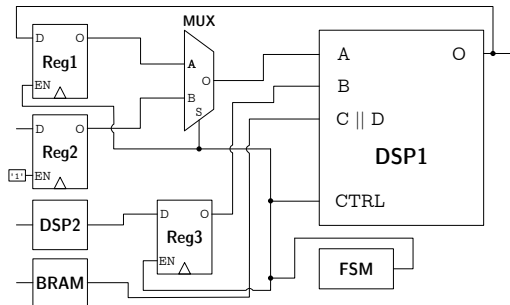


Figure 8: Simplified DSP circuit.

For each step of these sequences, we leveraged simulation to (i) analyze control inputs and the internal DSP state to determine the executed arithmetic operation and (ii) identify the data sources which the operands of this operation came from. The operands may have passed through MUXes and can originate from communication interfaces, registers, BRAMs, or other DSPs. We also encountered feedback loops when a DSP output is stored in a register that is again applied as an input to the same DSP later on, see Reg1 of Figure 8. Please note that we ignored the actual operand values, but rather traced their data sources to reconstruct symbolic equations describing the executed operations.

For this, we started at the inputs of the respective DSP. Whenever encountering a combinational structure such as a word-level MUX, we looked at the current value of its select signal in simulation to determine the selected data path. Sequential components add another dimension in that they require knowledge of past circuit states, which blows up complexity of static analysis. However, we could leverage information from simulation to avoid investigating all possible circuit states. For registers, we determined the simulation cycle in which they were last written and continued traversal from there. We proceeded with this manual approach until we reached another DSP, a memory, or a communication interface. By applying this to all four DSPs, we generated equations describing Maggie’s data path. Using these equations, we crafted a Python script that

replicates the algorithm implemented by the data path and verified correctness by checking against recorded outputs.

3.4 Step 4: High-Level Sense-Making

Based on the recovered algorithm, we proceeded with a semantic analysis that is essential for meaningful interaction with Apple’s IP. Generating a Python script implementing the algorithm proved crucial, since comprehending the algorithm required domain knowledge that was beyond our FPGA reverse engineering team. This way, we could share the Python script containing the reconstructed algorithm with a signal processing expert without requiring them to have any knowledge of the reverse engineering process.

Big Picture. Maggie is a central component of the iPhone 7 haptics subsystem to which Apple refers as *Taptic Engine*. We found that it controls the excitation of the linear resonant actuator (LRA) to produce a vibration which is perceived by the user as a tactile stimulus. For instance, the Taptic Engine creates the sensation of a physical button push for the non-mechanical home button of the iPhone 7. To provide such refined tactile feedback, a closed-loop control system is utilized which makes the LRA accurately follow a desired movement. Here, Maggie implements the closed-loop motion controller, see Figure 9 for a simplified block diagram, which conditions the drive signals applied to the actuator (via the motor driver) based on sensor feedback from the actuator itself.

Signal Processing. To generate the LRA control signals, Maggie operates on two feedback signals from the LRA, a reference signal previously loaded into BRAM, and values of intermediate signals at previous sampling instants. From the algorithmic representation, we identified several classical biquad filter stages implemented in a direct form I structure [54]. Upon closer inspection, we found many typical DSP building blocks, e.g., sub-sampling and sample-and-hold blocks for sample rate conversion, bit shifts and truncations for fixed-point arithmetic, saturation stages to prevent overflows, and filter implementations. Furthermore, we recognized even subtle details such as the use of *fraction saving* [75]. Putting it all together, we found three main processing stages: (i) input signal conditioning and application of calibration, (ii) a state observer to track the actuator dynamics, and (iii) the closed-loop controller to minimize errors between the actual and the desired LRA movement. For details on the recovered DSP operations, see Appendix B.

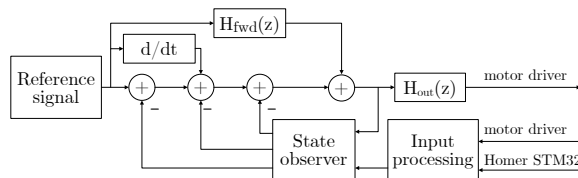


Figure 9: Overview of Maggie’s signal processing.

4 DERIVING GENERALIZED TECHNIQUES

Our case study demonstrated that a semi-automated approach for FPGA reverse engineering in the context of IP theft entails considerable effort. In line with RQ2, we now investigate whether (and

to what extent) the learnings from our case study can be generalized across different FPGA architectures. Upon publication, we will provide open-source implementations of our generalized tools.

We evaluated the techniques discussed in this section on six benchmark designs synthesized for Xilinx 7-series and Lattice iCE40 FPGAs, see Table 2 for evaluation results and Appendix C for details on the benchmarks. Furthermore, we conducted an end-to-end white-box case study on one signal processing design implemented for Xilinx 7-series FPGAs to showcase the effectiveness of our generalized techniques in concert.

4.1 Netlist Pre-Processing

So far, our pre-processing steps were limited to the 4-input LUTs found on Lattice iCE40 FPGAs. While some techniques such as the detection of duplicate gates could easily be extended to cover arbitrary combinational gates, this is not true for our LUT decomposition. Here, our approach works reasonably well for 4-input LUTs but does not scale to six inputs. Hence, for generalization, we re-synthesize the combinational subgraphs between sequential gates using open-source EDA tools instead of analyzing each LUT’s Boolean function. To this end, we constrain the synthesizer to a custom gate library comprising only the desired combinational gates such as AND, OR, XOR, and MUX of various sizes. Compared to decomposing the combinational parts of the netlist into a pure and-or-invert (AOI) graph, this approach allows us to delegate multiplexer (MUX) detection to the synthesizer by incentivizing the selection of MUX gates over alternatives by artificially reducing their size and optimizing for area. This way, we can even identify MUXes within complex LUT configurations. By nature, this re-synthesis approach is independent of the underlying FPGA architecture and target implementation.

Evaluation. We verified the correctness of our pre-processing using SMT solving. However, pre-processing is a best-effort approach and lacks a ground truth to compare against. It is essential for subsequent techniques such as word-level MUX detection and arithmetic structure identification. The success of these techniques serves as a proxy to gauge the effectiveness of our pre-processing approach.

4.2 Arithmetic Structures

In our case study, we identified arithmetic operations by building candidate sets of gates and verifying their function using an SMT solver. However, utilizing an SMT solver to compare against functional models from a library of known operations requires knowledge of the order of input and output signals as well as their operand membership. Furthermore, identifying any existing control signals presents additional challenges. When analyzing Maggie, we inferred operands of arithmetic operations from structural properties such as the pins of carry gates, e.g., operand A of an addition $A + B$ would often be connected to input I_0 of a Lattice iCE40 CARRY gate. The bit order of arithmetic operations was deduced from the structure of the underlying carry chains. This approach is similar to an idea proposed by Narayanan et al. [49]. However, such structural properties always depend on the particular implementation, FPGA architecture, surrounding logic, and synthesizer optimizations, hence calling for a more generic solution.

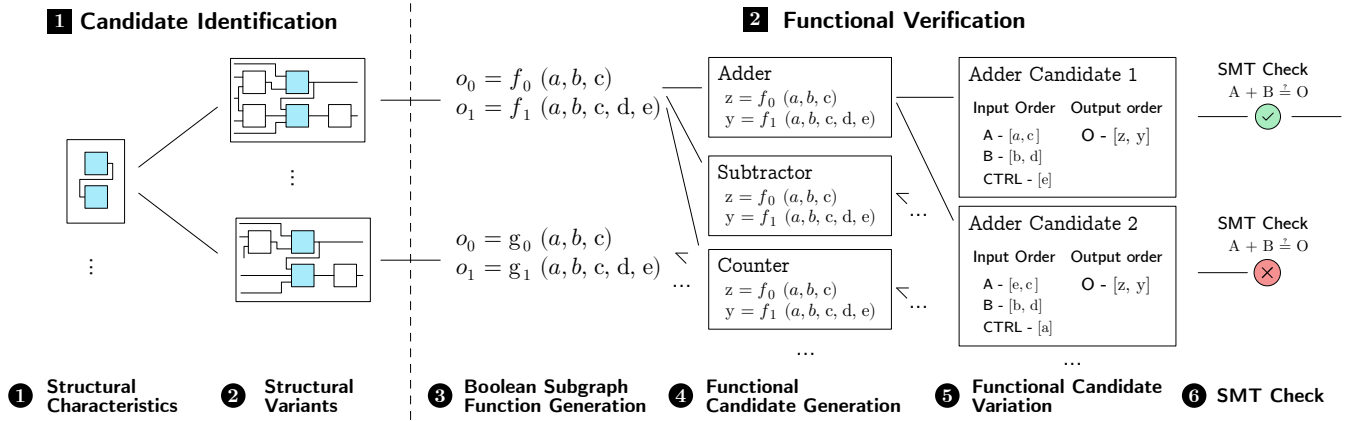


Figure 10: Module Identification and Classification Overview.

To address this issue, we developed a two-phased approach: We **1** identify candidates using architecture-dependent structural techniques and then **2** attempt to determine the functionality of each candidate using architecture-independent functional analysis. We move the challenge of identifying operands and their bit order to the second stage, hence making it architecture agnostic.

1 Candidate Identification. Arithmetic operations are often implemented using carry gates for both Xilinx and Lattice FPGAs. Because the characteristics of these carry gates can substantially differ between vendors, different approaches for structural candidate identification are required depending on the FPGA architecture. We **1** start from specific structural patterns in the netlist, such as carry chains, and then **2** generate the final candidates by additionally considering varying sets of preceding and succeeding combinational gates. We do this because the neighboring combinational logic can differ vastly depending on the implemented arithmetic operation and the number of control inputs.

A salient advantage of this methodology is its generic nature, which relieves the user of the intricate task of manually crafting exact candidates. So far, we implemented this structural approach for both Xilinx and Lattice iCE40 platforms. To integrate other FPGA architecture, the structural characteristics of that architecture must be investigated and techniques to compile structural candidates must be implemented. This can be done in a matter of hours.

2 Functional Verification. Having identified structural candidates, we attempt to determine their implemented operations using functional methods to remain architecture-agnostic. We first determine bit order, operand memberships, and control signals for each structural candidate. Afterwards, we check against a library of functional models of known arithmetic operations using an SMT solver.

To this end, we first **3** derive Boolean functions for all output nets from the sub-graph of each structural candidate. Next, **4** multiple different functional candidates are generated from the Boolean functions of each structural candidate to enable checking against different models from the library such as additions, subtractions, or comparisons. Since the identification of operands, control inputs, and bit orders may be ambiguous, **5** multiple variations of every

functional candidate are created. To reduce the number of variations, we leverage different functional characteristics depending on the operation to check for. For example, for adder input bit orders, we consider how many output nets are influenced by each input signal. The LSB of an adder influences all of its outputs, while the MSB usually influences only a single output. Similarly, for an adder’s output order, we consider how many inputs each output depends on. Here, the LSB depends on the least amount of inputs while the MSB depends on the most. Similar properties can be identified for other arithmetic operations. For each functional candidate and its variations, **6** we query an SMT solver to identify the functionality of the structures given different assignments to their control values.

Evaluation. We verified functionality under at least one control assignment for 94% of the carry chains across our benchmarks, see Table 2. Issues only arose when carry chains were strongly interwoven with surrounding control and data-path logic, which sometimes prevented extraction of correct structural candidates. Depending on the benchmark, we automatically verified that 1% to 91% (average: 32%) of all combinational gates implement an arithmetic operation. The variation in coverage is the result of different kinds of benchmark implementations. For signal processing designs like the `canny_edge_detector` and the `fft64`, the data path mostly comprises of arithmetic operations. CPU implementations such as `ibex`, `icicle`, and `simple_risc_v` contain fewer carry chains and more control logic, which explains lower numbers in detected arithmetic operations and overall combinational coverage.

4.3 Data Path

The idea behind the dataflow analysis methodology of DANA [1] is, by nature, independent of the target gate type. In our case study, we leveraged DANA to identify registers and developed a separate, but related, technique to group MUX gates into word-level structures. Similar to DANA, we used control signals as well as predecessor and successor gates to identify word-level MUXes. Accordingly, to generalize our data-path analysis, we extended DANA to take on arbitrary, user-defined gate types, including MUXes, instead of refining our initial approach. In addition, we added the option to provide known word-level structures of any kind to DANA to support

word-level recovery of the target gate type. For example, in our case study DANA could only search for registers and only previously identified registers could be provided as known groups. Now, DANA can also reconstruct word-level MUXes while taking previously identified registers and arithmetic operations into account.

Evaluation. To evaluate the success of register recovery, we followed the evaluation proposed for DANA [1]. We generated a ground truth by leveraging symbols left in the gate-level netlists of our benchmark by the synthesizer. Then, we use normalized mutual information (NMI) and purity as metrics to compare our refined approach against the original DANA implementation. To this end, we fed known word-level structures such as BRAMs, DSPs, and arithmetic operations to DANA as additional predefined knowledge to take into account during analysis. This marginally improved NMI and purity for most benchmarks, raising the NMI by up to 0.14 and the purity by up to 0.30, see Table 2.

We also employed DANA to recover word-level MUXes. However, by nature, no ground truth for MUXes exists, as they are implicitly created from HDL control flow structures by the synthesizer and then implemented in LUTs alongside other logic. Therefore, it is, at best, ambiguous which HDL constructs would be translated into a MUX and accurately measuring the quality of our results is impossible. Still, we provide an intuition for their quality by investigating the sizes of recovered MUXes in Appendix D.

4.4 Bit Order

Transferring our bit-order propagation algorithm from the case study to other FPGA architectures was straightforward because the algorithm was already generic by nature. It operates only on known pin groups of recovered structures and the netlist graph representation to determine successor and predecessor pin groups, which is applicable independent of the underlying gate types. However, CPU netlists tend to confuse our algorithm due to the interwoven data path of ALUs. To improve bit-order propagation results, we extended our approach for consensus-finding between conflicting bit orders propagated to the same pin group. To this end, we now apply three consensus-finding mechanisms that try to recover a consecutive bit order.

Consider a module with a group of three input pins $[i_0, i_1, i_2]$. After propagating pin indices from structures with known bit orders to those with unknown bit orders, each pin is annotated with multiple index candidates coming from different sources. Here, $[0, 1, 2]$ is a list of indices gathered from the same source structure, denoting that i_0 should receive index 0, i_1 index 1, and i_2 index 2. We use $?$ to indicate missing index information for the respective pin and X to show that the respective pin is no longer considered.

Shifted Consensus. If conflicting pin orders are propagated to the pins of a pin group, but these orders are just shifted variants of each other, consensus is found and an order starting at index 0 is annotated. For example, if orders $[1, 2, 3]$ and $[2, 3, 4]$ are propagated to a group of three pins, the pins will be assigned the order $[0, 1, 2]$.

Majority Consensus. If the propagated pin orders of a pin group are in conflict, but a non-conflicting majority vote on each individual pin is feasible, the predominant bit order is annotated. For example, if order $[0, 1, 2]$ is propagated to a group twice and order $[4, 3, 7]$ is

propagated once, $[0, 1, 2]$ is annotated by majority decision. Since index propagation is performed for each pin individually, there may not be a predominant index for every pin of a pin group. If the majority vote fails for a single pin of a group, no index is annotated to any pin of that group.

Iterative Majority Consensus. Sometimes, the same pin group index is propagated to multiple pins of the same group. For example, the order $[0, ?, 2]$ may be propagated to a group twice and order $[?, 1, 1]$ once. Here, the annotated indices $[?, 1, 1]$ will be ignored in the first iteration since they contain the same index for different pins of the same group, therefore conflicting with itself. Instead, indices 0 and 2 will be annotated to the first and the last pin by majority vote. In the second iteration, only the pins missing an index are considered. The previously gathered groups of indices $[0, ?, 2]$ and $[?, 1, 1]$ are now transformed into $[X, ?, X]$ and $[X, 1, X]$, thereby resolving internal conflicts. Now $[X, ?, X]$ and $[X, 1, X]$ cause the second pin to be annotated with index 1, finally resulting in $[0, 1, 2]$.

Evaluation. To evaluate our bit-order propagation, we considered the bit orders given for DSPs and BRAMs and the ones recovered for operands of arithmetic operations to be correct and started propagation from there. A reliable bit-order ground truth—given as labels left by the synthesizer—is only available for registers. For evaluation, we created registers based on the ground truth used to evaluate DANA. Furthermore, we only consider registers containing more than three FFs, as smaller ones often belong to the control path. In Table 2, we report the absolute number of pin groups we consider for bit-order propagation, the share of initially ordered pin groups, and the total share of ordered pin groups after propagation. In addition, we report the proportion of ordered pin groups that are correct according to our ground truth. On average, we reconstructed 86% of bit orders across our benchmarks with 97% of them being correct, demonstrating the effectiveness of our method. In line with expectations, we observed that the quality of bit-order propagation results improved with the number of structures featuring an inherently known bit order.

4.5 Guided Symbolic Execution

Manually tracing signals across clock cycles in simulation to identify the sources of DSP inputs in our case study turned out not to be scalable as it is tedious and error-prone, emphasizing the need for automation. Hence, we implemented a symbolic execution (SE) approach that is guided by concrete control values obtained from virtual probing or simulation to avoid state explosion. This approach can be helpful beyond DSP analysis to semi-automatically investigate a circuit's dynamic behavior.

Our approach allows symbolically evaluating any data signal and tracing it back to its origin to automatically generate equations describing that signal's behavior over time. These equations depend only on previously defined endpoints such as global inputs, constants (e.g., from memory), or registers. Thus, guided symbolic execution produces a system-level representation that abstracts away timing behavior and instead focuses on the sequence of computations. Finally, the human reverse engineer can manually simplify and interpret the extracted equations to assign high-level meaning.

Starting at the cycle of interest, our guided SE approach first constructs the Boolean function describing the combinational sub-graph in front of a net. Next, it replaces all previously identified control signals with concrete values from simulation while keeping all other variables symbolic. Each variable left in the Boolean function now corresponds to an output net of a sequential gate. If the sequential gate is not one of our endpoints, it finds the last cycle in which the gate was updated and continues back-tracing from the data inputs of the gate at that cycle. This process is repeated until the resulting Boolean function only contains variables corresponding to the output nets of our endpoints. To resolve potential recursive dependencies, our guided SE approach introduces intermediate variables to break up these dependencies when they are detected. To achieve this, we automatically identify sequential loops within the netlist and assign intermediate variables to the registers at the outputs of these loops.

Evaluation. Applying guided SE is highly specific to the target implementation and the goals of the reverse engineer. Therefore, it is impossible to express its effectiveness in numbers. Still, we applied guided SE in a white-box case study and verified the results against a ground truth in Section 4.6 to demonstrate correctness. In a second evaluation step, we applied guided SE on the Maggie netlist to highlight its efficiency and scalability. To this end, we semi-automatically extracted a Python script describing the circuit’s algorithmic behavior during execution, after initially performing the same task manually in Section 3.3. Thereby, we reduced the required effort from multiple weeks to merely a matter of days.

4.6 White-Box Case Study

To assess the applicability of our workflow, we conducted a white-box case study on a signal-processing design similar to Maggie. This additional study is conducted because it enables a comparison between the recovered design against a known ground truth, which is impossible in the black box setting. To this end, we synthesized an open-source Hilbert transformer design [53] for a Xilinx 7-series FPGA and then extracted an algorithmic abstraction from the resulting gate-level netlist using only our generalized techniques.

Word-Level Reconstruction. The initial netlist comprised 425 combinational and 619 sequential gates. After netlist pre-processing, we ended up with 1025 gates in total, 374 of them combinational and 651 sequential. Next, we recovered word-level structures using our generalized algorithms. The algorithm classified all 17 carry chains into 10 subtractions and 7 additions, identified 31 16-bit registers, and annotated 135 multi-bit pin groups to registers and arithmetic structures. When comparing against the ground truth, DANA achieved an NMI of 0.99, and our bit-order propagation assigned a correct bitorder to all pin groups. In total, we automatically assigned over 90% of all gates to word-level structures.

Algorithmic Recovery. The Hilbert transformer comes with a testbench to validate its Verilog description before implementation. The same testbench can also be used to simulate the gate-level netlist, thereby generating traces similar to those that we received from virtual probing in Section 3.3. We successfully identified all relevant control signals in the netlist by searching for nets connecting to the control pins of registers, as this is a precondition to

run guided SE effectively. Next, we fed concrete values generated through simulation with the provided testbench to our guided SE algorithm for all identified control signals. Finally, our guided SE approach generated a word-level Boolean function for each global output that only depends on global inputs and the aforementioned intermediate variables introduced because of recursion.

High-Level Sensemaking. We manually translated the recovered Boolean functions into Python code, which we again handed to a domain expert who was unaware of the nature of the analyzed design. The expert identified the high-level functionality from the script and drew a block diagram that largely matched the one provided in the official documentation, see Appendix E for a comparison.

Overall, our generalized techniques enabled us to recover a high-level functional description of the analyzed design in only a few days, a task that took months to complete for the iPhone netlist. Still, significant manual effort is required despite this speedup. Overall, this white-box case study allowed us to validate the results of our workflow against a ground truth, proving its effectiveness. Furthermore, the verified success in this white-box case study supports the correctness of the analogous black-box case study, which cannot be directly verified in the same manner because the black-box setting precludes the existence of a known ground truth.

5 DISCUSSION

5.1 Revisiting Research Questions

RQ1. In our case study, we successfully recovered the algorithm controlling the Taptic Engine of the iPhone 7. In response to RQ1, we now provide insights into the effort required to commit IP theft.

While netlist recovery was solved following a known path with suitable open-source tooling, netlist analysis presented challenges that took months to complete. In particular, the lack of hierarchy (C1), loss of data types (C2), and synthesizer optimizations (C3) initially hampered structural analysis, but could be dealt with once patterns were identified. This was achieved through an interplay of manual and automated reverse engineering by first searching for repeating structures and then systematically automating the detection thereof. While we automated substantial parts of the word-level reconstruction, manual inspection and correction were inevitably necessary to interpret results and address errors.

Classification of control logic (C4) had to be mostly done by hand as existing techniques provided limited insights, see Section 3.2. In the end, we bypassed in-depth analysis of FSM state graphs and their interplay with the data path and other FSMs by relying on virtual probing. Obtaining the I/O recordings required for this purpose presented engineering challenges on its own, see Figure 7, but these are situational and depend on the PCB. The main challenge for recovering the implemented algorithm was understanding the dynamic circuit behavior (C6), which almost entirely depended on external data (C5). To this end, simulation results were manually analyzed over many weeks. Finally, understanding the implemented algorithm required domain knowledge beyond our reverse engineering expertise (C7) and called for a signal processing expert.

Throughout our case study, validating intermediate results within the black-box setting we were operating in presented another significant challenge. Subsequent stages always depended on previous

Table 2: Results of our evaluation on the open-source benchmarks described in Table 3 and Maggie.

Design	Vendor	addition	subtraction	counter	negation	const. mul.	comparator	unknown	total	classified	DANA (Registers)				Bit Order			
											NMI (org.)	NMI (our)	purity (org.)	purity (our)	no. of groups	initial ordered	final ordered	correct
ibex	Lattice	5	0	3	0	0	0	1	9	0.04	0.96	0.97	0.97	0.97	165	0.25	0.39	0.91
	Xilinx	3	0	0	0	0	0	3	6	0.01	0.98	0.98	0.96	0.97	148	0.16	0.86	1.00
icicle	Xilinx	1	1	4	0	0	0	1	7	0.05	0.91	0.95	0.94	0.95	345	0.79	0.90	0.84
	Lattice	3	0	6	0	0	1	0	10	0.12	0.86	0.94	0.90	0.94	112	0.31	0.62	0.94
simple_risc_v	Xilinx	3	1	4	0	0	2	0	10	0.07	0.97	0.99	0.98	0.98	117	0.29	0.91	1.00
	Lattice	2	1	4	0	0	6	1	14	0.13	0.98	0.99	0.98	0.97	136	0.32	0.95	1.00
canny_edge_detector	Xilinx	57	0	1	2	49	3	6	118	0.77	0.81	0.81	0.61	0.64	619	0.46	0.91	0.99
	Lattice	69	0	1	0	34	6	8	118	0.60	0.81	0.85	0.71	0.82	813	0.43	0.78	1.00
fft64	Xilinx	25	5	0	0	4	0	6	40	0.27	0.90	0.97	0.79	0.96	351	0.37	0.97	0.97
	Lattice	93	4	5	0	6	0	1	109	0.40	0.88	0.94	0.77	0.91	604	0.59	0.93	0.96
sha256	Xilinx	10	0	0	0	0	0	3	13	0.26	0.91	0.96	0.75	0.87	134	0.25	0.97	1.00
	Lattice	11	0	1	0	0	0	0	12	0.10	0.94	0.97	0.81	0.90	170	0.22	0.99	1.00
hilbert_transformer	Xilinx	7	10	0	0	0	0	0	17	0.91	0.85	0.99	0.68	0.98	126	0.43	1.00	1.00
	Lattice	7	10	0	0	0	0	0	17	0.89	0.90	0.99	0.74	0.96	126	0.46	1.00	1.00
maggie	Lattice	4	0	24	0	0	15	0	43	0.16	N/A	N/A	N/A	N/A	326	0.47	0.79	N/A

findings, risking error propagation. This concern was particularly pronounced during word-level reconstruction and algorithmic recovery, where our efforts often felt akin to groping in the dark. Identifying and tracing errors was sometimes impossible. While the SMT-based verification of arithmetic operations offered an initial anchor point, this alone could not fully resolve the issue. In this regard, insights derived from virtual probing played a crucial role in achieving end-to-end validation of our reverse engineering result. Virtual probing was also instrumental in interpreting the data flowing through Maggie, enabling us to generate plots of processed data and extract equations representing the implemented algorithm.

An overshadowing issue of the entire case study was the lack of adequate, openly available tooling to automatically investigate the recovered netlist at scale. Developing respective tooling, e.g., for netlist simulation, required immense efforts and was the main reason for many of the months spent on conducting the case study.

RQ2. In light of RQ2, we developed fully automated techniques that address many of the challenges we encountered in our case study. Furthermore, we demonstrated their applicability across FPGA architectures, particularly focusing on Lattice and Xilinx FPGAs. We chose Xilinx as our second evaluation platform as they are the market leader among FPGA vendors and their 7-series FPGAs exhibit higher complexity than the Lattice iCE40 device family.

Generalizing netlist pre-processing, data-path analysis, and bit-order reconstruction required only minor tweaks, as the techniques from our iPhone case study were already independent of the FPGA architecture. Here, we focused on addressing issues arising from different implementations ranging from CPUs to DSP designs.

While redesigning the functional arithmetic verification required significant effort and took months to complete, adding support for different architectures is now a matter of hours and only requires extending the structural candidate identification. Furthermore, we showed that the labor-intensive dynamic extraction of an algorithmic description from Maggie can be sped up by our guided SE approach. This significantly reduced the time to get from word-level to an algorithmic description to at most a couple of days.

Still, we noticed that the quality of the results of our techniques varied depending on the *kind* of implementation we analyzed. DSP designs similar to Maggie generally yield better results than CPUs, presumably because the data and control paths in DSP designs exhibit more structure. As DSP designs feature more arithmetic operations than, e.g., central processing units (CPUs), we identify larger parts of their combinational data path. CPUs leverage varying bits of a register for a wide range of arithmetic operations and thus have a more interwoven data path, which sometimes required us to adapt our techniques. In particular, introducing majority voting to the bit-order propagation improved results for CPU implementations.

One challenge, however, remains unsolved: the identification and separation of control logic, see Section 3.2. We avoided this issue by using dynamic analysis, but it may not always be applicable, as dynamic analysis often requires observing an operational system.

By generalizing our techniques across different FPGA architectures and implementations, we demonstrated that some of the netlist reverse engineering challenges we identified can be considered a one-time overhead. The respective tooling only has to be developed once and can then be applied across a broad range of targets. Consequently, we contribute to significantly reducing

the manual effort of FPGA netlist reverse engineering by providing open-source implementations of the techniques presented in this section, allowing for a more realistic evaluation of countermeasures.

5.2 FPGA Threats & Defenses

Threats of FPGA Reverse Engineering. We showcased the feasibility of reverse engineering a real-world FPGA design, even within the limitations of a resource-constrained academic setting. Compared to regular ICs, the entry bar to reverse engineering is much lower. Unlike FPGAs, for which reliable open-source bitstream documentation projects are readily available [3, 4], the extraction of a netlist from an IC requires complex tooling, expensive equipment, and specialized expertise for preparation, imaging, and image analysis [22, 38, 56, 70, 71]. Given these inherent challenges of IC reverse engineering, we assume that ICs are more likely to be targeted by sophisticated attackers with nation-state-level resources. In contrast, FPGAs are vulnerable to reverse engineering by less powerful adversaries. On top of that, extracting an error-free netlist is much easier for FPGAs than it is for ICs, since for the latter, error-prone sample preparation and image analysis is needed while error-free bitstream documentation is more straight-forward to achieve. A correctly recovered gate-level netlist enables techniques like virtual probing (and simulation in general) that are sensitive to errors in the netlist, thereby increasing the threat potential even further.

In addition to IP theft, large-scale reverse engineering efforts can also provide an entry point for hardware Trojan insertion given the reconfigurability of FPGAs [33, 65, 66]. Consequently, a natural defense against netlist extraction would be to *not* use FPGAs for sensitive IP altogether. We recognize that this is not a viable option in many cases, hence additional FPGA countermeasures should be considered to defend against IP theft and Trojan insertion.

Bitstream Protections. A first line of defense is to impede the extraction of a gate-level netlist. Proprietary bitstream formats may initially raise the bar for a reverse engineering attack, but given increasing automation, this may be overcome within a reasonable time. This is inevitable since the user will always be able to translate HDL designs into bitstreams using EDA tools. As offered by many FPGA vendors, robust cryptographic schemes can ensure bitstream confidentiality, integrity, and authentication. By encrypting and signing a bitstream, attacks such as IP theft are impeded. However, such bitstream protections are not always provided on low-cost FPGAs and legacy devices, which continue to be used for decades.

Netlist Protections. In light of recent attacks on bitstream encryption schemes [19, 46–48, 67, 68], further precautions must be taken to harden the netlist against static and dynamic analysis by deteriorating those netlist properties that facilitate automated reverse engineering. Effective netlist obfuscation must aim at preventing the recovery of word-level structures as these structures are crucial for further analysis [8]. Dynamic reverse engineering is key to achieve an algorithmic understanding of larger circuits. Hence, to harden against such analysis techniques, non-simulatable primitives such as physical unclonable functions (PUFs) [72] or partial reconfiguration [23, 23, 63] should be included in the design and merged into the control and data paths.

5.3 Related Work

Existing netlist reverse engineering techniques often only tackle isolated problems and have been evaluated on (sometimes outdated) open-source benchmarks rather than black-box designs. Hence, a comprehensive real-world case study is still lacking in the literature. For a summary of prior work, see Azriel et al. [7].

One research strand focuses on automated state registers recognition and FSM recovery [41–44, 61]. RELIC by Meade et al. [11, 43] rates the similarity of FF fan-in trees to determine state and non-state FFs. Chowdhury et al. [13] propose a graph neural network (GNN) base approach that can also separate control FFs from data. To identify known sub-circuits, functional [36, 37, 43, 64] and graph-similarity based approaches [24] have been proposed. WordRev by Li et al. [36] comprises methods to recover word-level structures for functional matching. Subramanian et al. [64] builds on their work to identify components such as adders, multipliers, counters, and registers. Albartus et al. introduced DANA [1] to identify high-level registers in a gate-level netlist. Meade et al. presented REBUS and REWIND to recover the datapath using similarity metrics comparable to RELIC [43]. Alrahis et al. [5] utilize GNN to determine for each gate whether it belonged to a module that implements known functionality. Narayanan et al. [49] also propose an identification of arithmetic operations by taking advantage of carry chains on FPGAs, as discussed in Section 4.2. Some work has been done to partition a netlist based on the interconnectivity of a cluster of gates. Werner et al. [73] evaluate the applicability of conventional graph clustering algorithms to circuits, while Hong et al. [30] search for partitions by optimizing an n-cut with a GNN.

5.4 Limitations and Future Work

Our case study, while focused on a single DSP design on a relatively small FPGA, still provides valuable insights. As we have shown in Section 4, our case study findings inform generalized techniques that are applicable to implementations across different architectures, designs, and sizes. Future research could build up on this work to explore more elaborate real-world designs on more complex FPGAs to further underline the threat potential of IP theft for FPGAs. Our work builds the foundation for such case studies by providing the techniques to dissect such a netlist at scale. Also, we have shown that there still is a need for better automated techniques for control logic extraction and analysis in gate-level netlists.

6 CONCLUSION

Our work highlights the challenges associated with IP theft through FPGA reverse engineering and discusses the issues arising in a real-world setting. To this end, our case study on a Lattice iCE40 FPGA that is part of iPhone 7 underscores the vulnerability of FPGAs to IP theft due to the low barrier for netlist extraction compared to regular ICs. Thereby, we reveal that while IP theft from FPGAs requires substantial effort, specialized skills, and domain knowledge, most labor-intensive steps can be automated. We contribute to the field by introducing generalized netlist reverse engineering techniques and open-source implementations, which reduce manual effort and facilitate future research in this domain. Our techniques prove effective across different FPGA architectures and highlight the threat of IP theft even by less resourceful adversaries. This

work emphasizes the importance of robust bitstream and netlist protections to safeguard valuable IP in FPGAs. Finally, we call for more open and transparent research in FPGA reverse engineering to better understand and mitigate associated threats.

ACKNOWLEDGMENTS

We thank Marc Fyrbiak and Max Hoffmann for the fruitful discussions. Funded by the Deutsche Forschungsgemeinschaft (DFG, German Research Foundation) under Germany's Excellence Strategy - EXC 2092 CASA - 390781972, through ERC grant 695022, NSF grants CNS-1563829 and CNS-1749845, and ISF project IZ25-5793-2019-43 (CHloSec).

REFERENCES

- [1] Nils Albartus, Max Hoffmann, Sebastian Temme, Leonid Azriel, and Christof Paar. 2020. DANA Universal Dataflow Analysis for Gate-Level Netlist Reverse Engineering. *IACR Trans. Cryptogr. Hardw. Embed. Syst.* 2020, 4 (2020), 309–336.
- [2] Chips Alliance. 2022. F4PGA. <https://f4pga.org>
- [3] Chips Alliance. 2023. Project IceStorm. <https://github.com/YosysHQ/icestorm>
- [4] Chips Alliance. 2023. Project X-Ray. <https://github.com/f4pga/prjxray>
- [5] Lilas Alrahis, Abhrajit Sengupta, Johann Knechtel, Satwik Patnaik, Hani H. Saleh, Baker Mohammad, Mahmoud Al-Qutayri, and Ozgur Sinanoglu. 2022. GNN-RE: Graph Neural Networks for Reverse Engineering of Gate-Level Netlists. *IEEE Trans. Comput. Aided Des. Integr. Circuits Syst.* 41, 8 (2022), 2435–2448.
- [6] angelobacchini OpenCores. [n. d.]. Canny Edge Detector VHDL. https://opencores.org/projects/canny_edge_detector
- [7] Leonid Azriel, Julian Speith, Nils Albartus, Ran Ginossar, Avi Mendelson, and Christof Paar. 2021. A survey of algorithmic methods in IC reverse engineering. *J. Cryptogr. Eng.* 11, 3 (2021), 299–315.
- [8] Giorgi Bashiashvili, Zail Ul Abideen, and Samuel Pagliarini. 2022. Obfuscating the Hierarchy of a Digital IP. *CoRR abs/2205.09892* (2022), 303–314.
- [9] S. Beale and B. Shafai. 1989. Robust control system design with a proportional integral observer. *Internat. J. Control* 50, 1 (1989), 97–111.
- [10] Florian Benz, André Seffrin, and Sorin A. Huss. 2012. Bil: A tool-chain for bitstream reverse-engineering. In *22nd International Conference on Field Programmable Logic and Applications (FPL), Oslo, Norway, August 29-31, 2012*, Dirk Koch, Satnam Singh, and Jim Torresen (Eds.). IEEE, Oslo, Norway, 735–738.
- [11] Michaela Brunner, Johanna Baehr, and Georg Sigl. 2019. Improving on State Register Identification in Sequential Hardware Reverse Engineering. In *IEEE International Symposium on Hardware Oriented Security and Trust, HOST 2019, McLean, VA, USA, May 5-10, 2019*. IEEE, McLean, VA, USA, 151–160.
- [12] Michaela Brunner, Alexander Hepp, Johanna Baehr, and Georg Sigl. 2022. Toward a Human-Readable State Machine Extraction. *ACM Trans. Design Autom. Electr. Syst.* 27, 6 (2022), 58:1–58:31.
- [13] Subhjit Dutta Chowdhury, Kaixin Yang, and Pierluigi Nuzzo. 2021. ReIGNN: State Register Identification Using Graph Neural Networks for Circuit Reverse Engineering. In *IEEE/ACM International Conference On Computer Aided Design, ICCAD 2021, Munich, Germany, November 1-4, 2021*. IEEE, Munich, Germany, 1–9.
- [14] damdoy. [n. d.]. RISC-V implementation on iCE40. https://github.com/damdoy/ice40_ultraplus_examples/tree/master/riscv
- [15] Zheng Ding, Qiang Wu, Yizhong Zhang, and Linjie Zhu. 2013. Deriving an NCD file from an FPGA bitstream: Methodology, architecture and evaluation. *Microprocess. Microsystems* 37, 3 (2013), 299–312.
- [16] George Ellis. 2002. *Observers in control systems: a practical guide*. Elsevier.
- [17] George Ellis. 2012. *Control system design guide: using your computer to understand and diagnose feedback controllers*. Butterworth-Heinemann.
- [18] Maik Ender, Gregor Leander, Amir Moradi, and Christof Paar. 2022. A Cautionary Note on Protecting Xilinx' UltraScale(+) Bitstream Encryption and Authentication Engine. In *30th IEEE Annual International Symposium on Field-Programmable Custom Computing Machines, FCCM 2022, New York City, NY, USA, May 15-18, 2022*. IEEE, New York City, NY, USA, 1–9.
- [19] Maik Ender, Amir Moradi, and Christof Paar. 2020. The Unpatchable Silicon: A Full Break of the Bitstream Encryption of Xilinx 7-Series FPGAs. In *29th USENIX Security Symposium, USENIX Security 2020, August 12-14, 2020*, Srdjan Capkun and Franziska Roesner (Eds.). USENIX Association, Virtual Event, 1803–1819.
- [20] Maik Ender, Pawel Swierczynski, Sebastian Wallat, Matthias Wilhelm, Paul Martin Knopp, and Christof Paar. 2019. Insights into the mind of a trojan designer: the challenge to integrate a trojan into the bitstream. In *Proceedings of the 24th Asia and South Pacific Design Automation Conference, ASPDAC 2019, Tokyo, Japan, January 21-24, 2019*, Toshiyuki Shibuya (Ed.). ACM, Tokyo, Japan, 112–119.
- [21] Domenic Forte, Swarup Bhunia, and Mark M Tehranipoor. 2017. *Hardware protection through obfuscation*. Springer.
- [22] Marc Fyrbiak, Sebastian Strauss, Christian Kison, Sebastian Wallat, Malte Elson, Nikol Rummel, and Christof Paar. 2017. Hardware reverse engineering: Overview and open challenges. In *IEEE 2nd International Verification and Security Workshop, IVSW 2017, Thessaloniki, Greece, July 3-5, 2017*. IEEE, Thessaloniki, Greece, 88–94.
- [23] Marc Fyrbiak, Sebastian Wallat, Jonathan Déchelotte, Nils Albartus, Sinan Böcker, Russell Tessier, and Christof Paar. 2018. On the Difficulty of FSM-based Hardware Obfuscation. *IACR Trans. Cryptogr. Hardw. Embed. Syst.* 2018, 3 (2018), 293–330.
- [24] Marc Fyrbiak, Sebastian Wallat, Sascha Reinhard, Nicolai Bissantz, and Christof Paar. 2020. Graph Similarity and its Applications to Hardware Security. *IEEE Trans. Computers* 69, 4 (2020), 505–519.
- [25] James Geist, Travis Meade, Shaojie Zhang, and Yier Jin. 2020. RELIC-FUN: Logic Identification through Functional Signal Comparisons. In *57th ACM/IEEE Design Automation Conference, DAC 2020, San Francisco, CA, USA, July 20-24, 2020*. IEEE, San Francisco, CA, USA, 1–6.
- [26] grahamedgecombe. [n. d.]. Icicle. <https://github.com/grahamedgecombe/icicle>
- [27] Arman Hajati. 2021. Electronic Device Including Multi-Phase Driven Linear Haptic Actuator and Related Methods.
- [28] Arman Hajati and Parin Patel. 2018. Electronic Device Including Closed-Loop Controller for Haptic Actuator and Related Methods.
- [29] HAL. 2018. HAL – The Hardware Analyzer. <https://github.com/emsec/hal>
- [30] Xuenong Hong, Tong Lin, Yiqiong Shi, and Bah-Hwee Gwee. 2023. GraphClusNet: A Hierarchical Graph Neural Network for Recovered Circuit Netlist Partitioning. *IEEE Trans. Artif. Intell.* 4, 5 (2023), 1199–1213.
- [31] iFixit. 2016. iPhone 7 Teardown. <https://de.ifixit.com/Teardown/iPhone+7+Teardown/67382>
- [32] Insider Monkey and Macrotrends. 2022. Ranking of the companies with the highest spending on research and development worldwide in 2022 (in billion U.S. dollars). <https://www.statista.com/statistics/265645/ranking-of-the-20-companies-with-the-highest-spending-on-research-and-development/>
- [33] Jatin Kataria, Rick Housley, Joseph Pantoga, and Ang Cui. 2019. Defeating Cisco Trust Anchor: A Case-Study of Recent Advancements in Direct FPGA Bitstream Manipulation. In *13th USENIX Workshop on Offensive Technologies (WOOT 19)*. USENIX Association, Santa Clara, CA, USA, 1–13. <https://www.usenix.org/conference/woot19/presentation/kataria>
- [34] Martin Kumm. 2008. Hilbert Transformator IP Cores. http://www.martin-kumm.de/wiki/lib/exe/fetch.php?media=FPGA_Cores:hilbert_transformer.pdf
- [35] Albert Zhichun Li. 2020. Intellectual Property Breaches Illustrate New Generation Of Security Threats. <https://www.forbes.com/sites/forbestechcouncil/2020/07/07/intellectual-property-breaches-illustrate-new-generation-of-security-threats/>
- [36] Wenchao Li, Adrià Gascón, Pramod Subramanyan, Wei Yang Tan, Ashish Tiwari, Sharad Malik, Natarajan Shankar, and Sanjit A. Seshia. 2013. WordRev: Finding word-level structures in a sea of bit-level gates. In *2013 IEEE International Symposium on Hardware-Oriented Security and Trust, HOST 2013, Austin, TX, USA, June 2-3, 2013*. IEEE Computer Society, Austin, TX, USA, 67–74.
- [37] Wenchao Li, Zach Wasson, and Sanjit A. Seshia. 2012. Reverse engineering circuits using behavioral pattern mining. In *2012 IEEE International Symposium on Hardware-Oriented Security and Trust, HOST 2012, San Francisco, CA, USA, June 3-4, 2012*. IEEE Computer Society, San Francisco, CA, USA, 83–88.
- [38] Bernhard Lippmann, Michael Werner, Niklas Unverricht, Aayush Singla, Peter Egger, Anja Dübotzky, Horst A. Gieser, Martin Rasche, Oliver Kellermann, and Helmut Graeb. 2019. Integrated flow for reverse engineering of nanoscale technologies. In *Proceedings of the 24th Asia and South Pacific Design Automation Conference, ASPDAC 2019, Tokyo, Japan, January 21-24, 2019*, Toshiyuki Shibuya (Ed.). ACM, Tokyo, Japan, 82–89.
- [39] lowrisc. [n. d.]. ibex RISC-V Core. <https://github.com/lowRISC/ibex>
- [40] John Martellaro. 2016. Thoughts About Apple's Secret iPhone 7 Chip. <https://www.macobserver.com/columns-opinions/editorial/apple-secret-iphone-7-chip/>
- [41] Kenneth S. McElvain. 2001. Methods and apparatuses for automatic extraction of finite state machines.
- [42] Travis Meade, Yier Jin, Mark Tehranipoor, and Shaojie Zhang. 2016. Gate-level netlist reverse engineering for hardware security: Control logic register identification. In *IEEE International Symposium on Circuits and Systems, ISCAS 2016, Montréal, QC, Canada, May 22-25, 2016*. IEEE, Montréal, QC, Canada, 1334–1337.
- [43] Travis Meade, Kaveh Shamsi, Thao Le, Jia Di, Shaojie Zhang, and Yier Jin. 2018. The Old Frontier of Reverse Engineering: Netlist Partitioning. *J. Hardware and Systems Security* 2, 3 (2018), 201–213.
- [44] Travis Meade, Shaojie Zhang, and Yier Jin. 2016. Netlist reverse engineering for high-level functionality reconstruction. In *21st Asia and South Pacific Design Automation Conference, ASP-DAC 2016, Macao, Macao, January 25-28, 2016*. IEEE, Macao, 655–660.
- [45] Travis Meade, Shaojie Zhang, and Yier Jin. 2018. NETA: Netlist Analysis Toolset. <https://github.com/jinyier/neta>

- [46] Amir Moradi, Alessandro Barenghi, Timo Kasper, and Christof Paar. 2011. On the vulnerability of FPGA bitstream encryption against power analysis attacks: extracting keys from xilinx Virtex-II FPGAs. In *Proceedings of the 18th ACM Conference on Computer and Communications Security, CCS 2011, Chicago, Illinois, USA, October 17-21, 2011*, Yan Chen, George Danezis, and Vitaly Shmatikov (Eds.). ACM, Chicago, Illinois, USA, 111–124.
- [47] Amir Moradi, Markus Kasper, and Christof Paar. 2012. Black-Box Side-Channel Attacks Highlight the Importance of Countermeasures - An Analysis of the Xilinx Virtex-4 and Virtex-5 Bitstream Encryption Mechanism. In *Topics in Cryptology - CT-RSA 20W12 - The Cryptographers' Track at the RSA Conference 2012, San Francisco, CA, USA, February 27 - March 2, 2012. Proceedings (Lecture Notes in Computer Science, Vol. 7178)*, Orr Dunkelman (Ed.). Springer, San Francisco, CA, USA, 1–18.
- [48] Amir Moradi and Tobias Schneider. 2016. Improved Side-Channel Analysis Attacks on Xilinx Bitstream Encryption of 5, 6, and 7 Series. In *Constructive Side-Channel Analysis and Secure Design - 7th International Workshop, COSADE 2016, Graz, Austria, April 14-15, 2016, Revised Selected Papers (Lecture Notes in Computer Science, Vol. 9689)*, François-Xavier Standaert and Elisabeth Oswald (Eds.). Springer, Graz, Austria, 71–87.
- [49] Ram Venkat Narayanan, Aparajithan Nathamuni Venkatesan, Kishore Pula, Sundarakumar Muthukumar, and Ranga Venuri. 2023. Reverse Engineering Word-Level Models from Look-Up Table Netlists. In *24th International Symposium on Quality Electronic Design, ISQED 2023, San Francisco, CA, USA, April 5-7, 2023*. IEEE, San Francisco, CA, USA, 1–8.
- [50] Dmitry Nedospasov, Jean-Pierre Seifert, Alexander Schlösser, and Susanna Orlic. 2012. Functional integrated circuit analysis. In *2012 IEEE International Symposium on Hardware-Oriented Security and Trust, HOST 2012, San Francisco, CA, USA, June 3-4, 2012*. IEEE Computer Society, San Francisco, CA, USA, 102–107.
- [51] Jean-Baptiste Note. 2008. debit. <https://github.com/djn3m0/debit>
- [52] Jean-Baptiste Note and Éric Rannaud. 2008. From the bitstream to the netlist. In *Proceedings of the ACM/SIGDA 16th International Symposium on Field Programmable Gate Arrays, FPGA 2008, Monterey, California, USA, February 24-26, 2008*, Mike Hutton and Paul Chow (Eds.). ACM, Monterey, California, USA, 264.
- [53] Martin Kumm OpenCores. [n. d.]. Hilbert Transformer VHDL. https://opencores.org/projects/hilbert_transformer
- [54] Alan V. Oppenheim and Ronald W. Schaffer. 2014. *Discrete-Time Signal Processing Third Edition*. Pearson Education Limited.
- [55] Khoa Dang Pham, Edson L. Horta, and Dirk Koch. 2017. BITMAN: A tool and API for FPGA bitstream manipulations. In *Design, Automation & Test in Europe Conference & Exhibition, DATE 2017, Lausanne, Switzerland, March 27-31, 2017*, David Atienza and Giorgio Di Natale (Eds.). IEEE, Lausanne, Switzerland, 894–897.
- [56] Shahed E. Quadir, Junlin Chen, Domenic Forte, Navid Asadizanjani, Sina Shahbazzamohamadi, Lei Wang, John A. Chandy, and Mark Tehranipoor. 2016. A Survey on Chip to System Reverse Engineering. *JETC* 13, 1 (2016), 6:1–6:34.
- [57] secworks. [n. d.]. SHA-256 verilog Core. <https://github.com/secworks/sha256>
- [58] Lattice Semiconductor. 2016. Lattice ICE Technology Library. https://www.latticesemi.com/-/media/LatticeSemi/Documents/TechnicalBriefs/SBTICETechnologyLibrary201608.ashx?document_id=51982
- [59] Anatolij Sergiyenko and Oleg Uzenkov. [n. d.]. Pipelined FFT/IFFT 64 points processor. https://opencores.org/projects/pipelined_fft_64
- [60] Kaveh Shamsi, Meng Li, Travis Meade, Zheng Zhao, David Z. Pan, and Yier Jin. 2017. AppSAT: Approximately deobfuscating integrated circuits. In *2017 IEEE International Symposium on Hardware Oriented Security and Trust, HOST 2017, McLean, VA, USA, May 1-5, 2017*. IEEE Computer Society, McLean, VA, USA, 95–100.
- [61] Yiqiong Shi, Chan Wai Ting, Bah-Hwee Gwee, and Ye Ren. 2010. A highly efficient method for extracting FSMs from flattened gate-level netlist. In *International Symposium on Circuits and Systems (ISCAS 2010), May 30 - June 2, 2010, Paris, France*. IEEE, Paris, France, 2610–2613.
- [62] Wilson Snyder. 2003. verilator. <https://github.com/verilator/verilator>
- [63] Florian Stolz, Nils Albartus, Julian Speith, Simon Klix, Clemens Nasenberg, Aiden Gula, Marc Fyrbiak, Christof Paar, Tim Güneysu, and Russell Tessier. 2021. Life-Line for FPGA Protection: Obfuscated Cryptography for Real-World Security. *IACR Trans. Cryptogr. Hardw. Embed. Syst.* 2021, 4 (2021), 412–446.
- [64] Pramod Subramanyan, Nestan Tsiskaridze, Kanika Pasricha, Dillon Reisman, Adriana Susnea, and Sharad Malik. 2013. Reverse engineering digital circuits using functional analysis. In *Design, Automation and Test in Europe, DATE 13, Grenoble, France, March 18-22, 2013*, Enrico Macii (Ed.). EDA Consortium San Jose, CA, USA / ACM DL, Grenoble, France, 1277–1280.
- [65] Pawel Swierczynski, Marc Fyrbiak, Philipp Koppe, Amir Moradi, and Christof Paar. 2017. Interdiction in practice - Hardware Trojan against a high-security USB flash drive. *J. Cryptogr. Eng.* 7, 3 (2017), 199–211.
- [66] Pawel Swierczynski, Marc Fyrbiak, Philipp Koppe, and Christof Paar. 2015. FPGA Trojans Through Detecting and Weakening of Cryptographic Primitives. *IEEE Trans. on CAD of Integrated Circuits and Systems* 34, 8 (2015), 1236–1249.
- [67] Pawel Swierczynski, Amir Moradi, David F. Oswald, and Christof Paar. 2015. Physical Security Evaluation of the Bitstream Encryption Mechanism of Altera Stratix II and Stratix III FPGAs. *ACM Trans. Reconfigurable Technol. Syst.* 7, 4 (2015), 34:1–34:23.
- [68] Shahin Tajik, Heiko Lohrke, Jean-Pierre Seifert, and Christian Boit. 2017. On the Power of Optical Contactless Probing: Attacking Bitstream Encryption of FPGAs. In *Proceedings of the 2017 ACM SIGSAC Conference on Computer and Communications Security, CCS 2017, Dallas, TX, USA, October 30 - November 03, 2017*, Bhavani M. Thuraisingham, David Evans, Tal Malkin, and Dongyan Xu (Eds.). ACM, Dallas, TX, USA, 1661–1674.
- [69] Aaron Tilley. 2016. This Mysterious Chip In The iPhone 7 Could Be Key To Apple's AI Push. <https://www.forbes.com/sites/aarontilley/2016/10/17/iphone-7-fpga-chip-artificial-intelligence/?sh=6268ab013c69>
- [70] Randy Torrance and Dick James. 2009. The State-of-the-Art in IC Reverse Engineering. In *Cryptographic Hardware and Embedded Systems - CHES 2009, 11th International Workshop, Lausanne, Switzerland, September 6-9, 2009, Proceedings (Lecture Notes in Computer Science, Vol. 5747)*, Christophe Clavier and Kris Gaj (Eds.). Springer, Lausanne, Switzerland, 363–381.
- [71] Randy Torrance and Dick James. 2011. The state-of-the-art in semiconductor reverse engineering. In *Proceedings of the 48th Design Automation Conference, DAC 2011, San Diego, California, USA, June 5-10, 2011*, Leon Stok, Nikil D. Dutt, and Soha Hassoun (Eds.). ACM, San Diego, California, USA, 333–338.
- [72] James B. Wendt and Miodrag Potkonjak. 2014. Hardware obfuscation using PUF-based logic. In *The IEEE/ACM International Conference on Computer-Aided Design, ICCAD 2014, San Jose, CA, USA, November 3-6, 2014*, Yao-Wen Chang (Ed.). IEEE, San Jose, CA, USA, 270–277.
- [73] Michael Werner, Bernhard Lippmann, Johanna Baehr, and Helmut Gräß. 2018. Reverse Engineering of Cryptographic Cores by Structural Interpretation Through Graph Analysis. In *3rd IEEE International Verification and Security Workshop, IVSW 2018, Costa Brava, Spain, July 2-4, 2018*. IEEE, Costa Brava, Spain, 13–18.
- [74] Jianhua Wu, Yong Han, Zhenhua Xiong, and Han Ding. 2017. Servo performance improvement through iterative tuning feedforward controller with disturbance compensator. *International Journal of Machine Tools and Manufacture* 117 (2017), 1–10.
- [75] Randy Yates and Richard Lyons. 2008. DC Blocker Algorithms [DSP Tips & Tricks]. *IEEE Signal Processing Magazine* 25, 2 (2008), 132–134.
- [76] Daniel Ziener, Stefan Assmus, and Jürgen Teich. 2006. Identifying FPGA IP-Cores Based on Lookup Table Content Analysis. In *Proceedings of the 2006 International Conference on Field Programmable Logic and Applications (FPL), Madrid, Spain, August 28-30, 2006*. IEEE, Madrid, Spain, 1–6.

A SIMULATION IN HAL

For netlist simulation in HAL, e.g., in the context of virtual probing, we extended the framework with an interface for commercial-grade simulation tools such as Verilator [62]. Furthermore, we added a waveform viewer to the HAL GUI that can be controlled via a Python API, see Figure 13. The dynamic state of the netlist can also be represented by coloring the nets in the graph view according to their current signal value, which adapts whenever the cursor in the waveform viewer is moved. See Figure 11 and Figure 12 for pictures of our actual virtual probing setup as initially described in Figure 7.

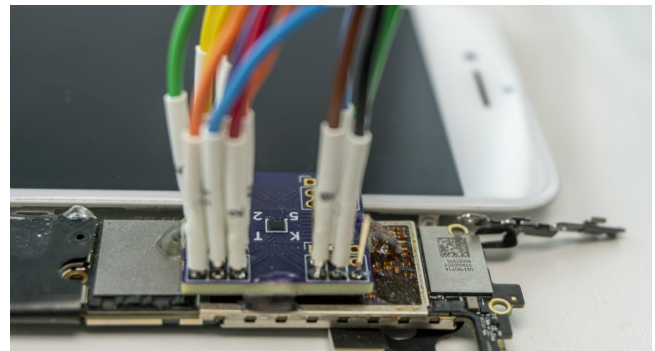


Figure 11: Side view of our custom breakout board sitting between the iPhone PCB and Maggie.

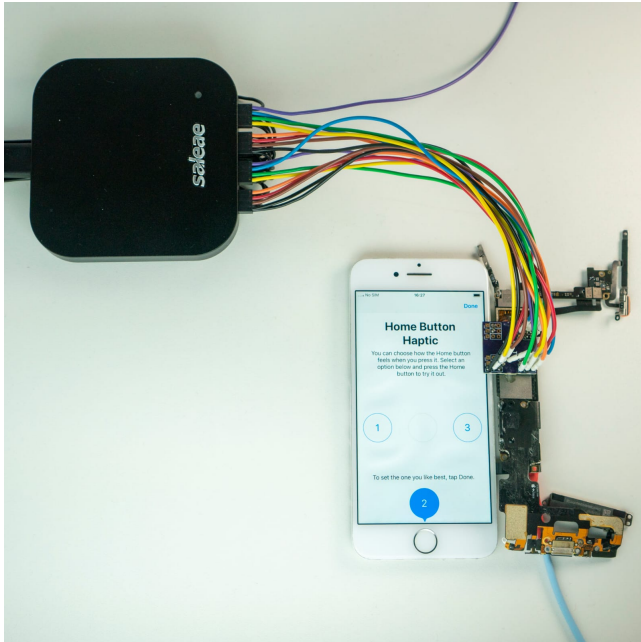


Figure 12: Top view of a Saleae logic analyzer being connected to the iPhone via our custom breakout board.

B DETAILS ON THE MAGGIE DSP

In the following, we briefly comment on three key building blocks of the DSP implementation, as shown in Figure 9: (i) an input processing, (ii) a state observer to track the actuator dynamics, and (iii) a closed-loop controller making the actuator follow a desired movement.

Input Processing. Maggie’s data path takes two input signals supplied via I²S and SPI from the motor driver and Homer, respectively. These two signals are combined (scaled and subtracted) and then passed to a look-up table-based function where linear interpolation is used to enhance resolution. We believe that this step translates sensor measurements to the current LRA position, relying on calibration.

State Observer. The input processing result and the closed-loop controller output are passed to a processing stage which implements a state observer, estimating the LRA’s position and velocity. In particular, Maggie appears to implement a proportional-integral (PI) observer [9].

Closed-Loop Controller. The closed-loop controller takes a time series of desired actuator positions as its reference signal. Thus, as different haptic events are to be generated, this signal is changed. For instance, it is updated with the haptic feedback setting visible in Figure 12. Using the reference signal and the state observer outputs, the closed-loop controller accumulates the position and the velocity error (the desired velocity is obtained from numerical differentiation of the reference signal) and subtracts the integrated

position estimation error. The particular combination of error components suggests that the control loop is a proportional-integral-derivative (PID)-controller [16, 17, 74]. Before being passed to the motor driver via I²S, a low-pass filter is applied to the output of the closed-loop controller.

C BENCHMARKS

Table 3 depicts the resource utilization of our six benchmark designs. Differences in resource utilization between the Xilinx and Lattice benchmarks, e.g., for `fft64`, can be the result of the Xilinx synthesizer using DSPs where the Lattice synthesizer resorts to carry chains. Furthermore, Xilinx FPGAs leverage 6-input LUTs while Lattice FPGAs use 4-input ones.

Table 3: Open-source benchmark resource utilization in the number of gates.

Design	Vendor	LUT	Carry	FF	BRAM	DSP	Other	Total
<code>ibex</code> [39]	Xilinx	3503	65	1937	0	1	727	6233
	Lattice	6379	295	1963	16	0	78	8731
<code>icicle</code> [26]	Xilinx	1525	65	1009	270	0	78	2947
	Lattice	2705	262	983	20	0	59	4029
<code>simple_risc_v</code> [14]	Xilinx	1617	76	1003	6	0	37	2739
	Lattice	2876	274	1235	6	0	31	4422
<code>canny_edge_detector</code> [6]	Xilinx	2538	636	3713	24	0	72	6983
	Lattice	3298	2170	4484	32	0	68	10052
<code>fft64</code> [59]	Xilinx	1722	212	1988	3	4	160	4089
	Lattice	5362	2008	2556	14	0	124	10064
<code>sha256</code> [57]	Xilinx	2196	104	1830	0	0	269	4399
	Lattice	3935	346	2378	0	0	90	6749
<code>hilbert_transformer</code> [53]	Xilinx	304	68	587	0	0	85	1044
	Lattice	445	225	569	2	0	78	1349
<code>maggie</code>	Lattice	3241	422	1342	18	4	19	5046

D MUX EVALUATION

MUXes of sizes that divide the bit-size of the datapath or are multiples of a byte are likely to be correct. To this end, we plotted the distributions of the top 5 MUX sizes for all benchmarks in Figure 14. The figure illustrates the five most frequently recovered MUX sizes for each benchmark, once synthesized for a Xilinx 7-series FPGA and once for a Lattice iCE40 FPGA. In this analysis, we exclusively consider MUXes comprising at least four gates. For the `hilbert_transformer`, no word-level MUXes were identified, hence we omitted it in Figure 14. We also provide our results for Maggie, which are only available for Lattice.

E WHITE-BOX CASE STUDY COMPARISON

In our white-box case study, we used an open-source Hilbert transformer design [53] as the ground truth to validate our generalized techniques. A signal processing expert unaware of the nature of the analyzed design inspected the Python code representing the recovered Boolean functions to draw a block diagram. From their analysis, they correctly identified the Hilbert transformer. Figure 15 shows the block diagrams representing the implemented signal processing chain. The diagram recovered from the gate-level netlist is shown in Figure 15a and the one taken from the implementation’s documentation [34] in Figure 15b. While the recovered block

diagram largely resembles the one from the documentation, partially matching exactly, there are also notable differences. Some are due to visualization choices, e.g., in favor of symmetry in the lower signal path, and others are due to implementation details affecting intermediate signals. For example, delay elements (represented by negative powers of z) can easily be moved around by factoring them into or out of parts of the processing. Similarly, delay elements that simply shift the entire output signal may be

added or removed without altering the time-invariant processing behavior. Furthermore, the trivial addition with 0 denoted in the documentation (first dashed box labeled $C_{+90}(z)$ in Figure 15b) is not found in the netlist, likely due to synthesizer optimizations. Please note that, despite the deviation of the visual representations and minor trivial differences, both block diagrams still describe the same overall processing.

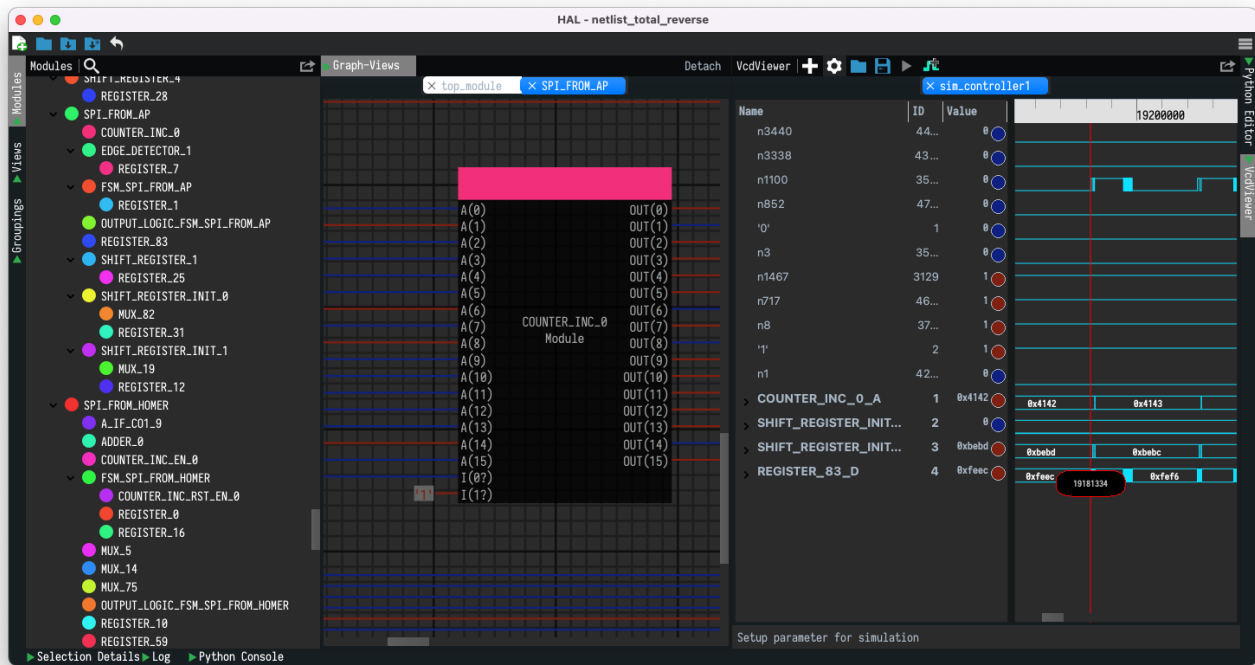


Figure 13: Screenshot of HAL showing the module tree on the left, the graph view in the middle, and the simulator on the right. The nets are colored depending on their current value, blue represents a 0 and red a 1.

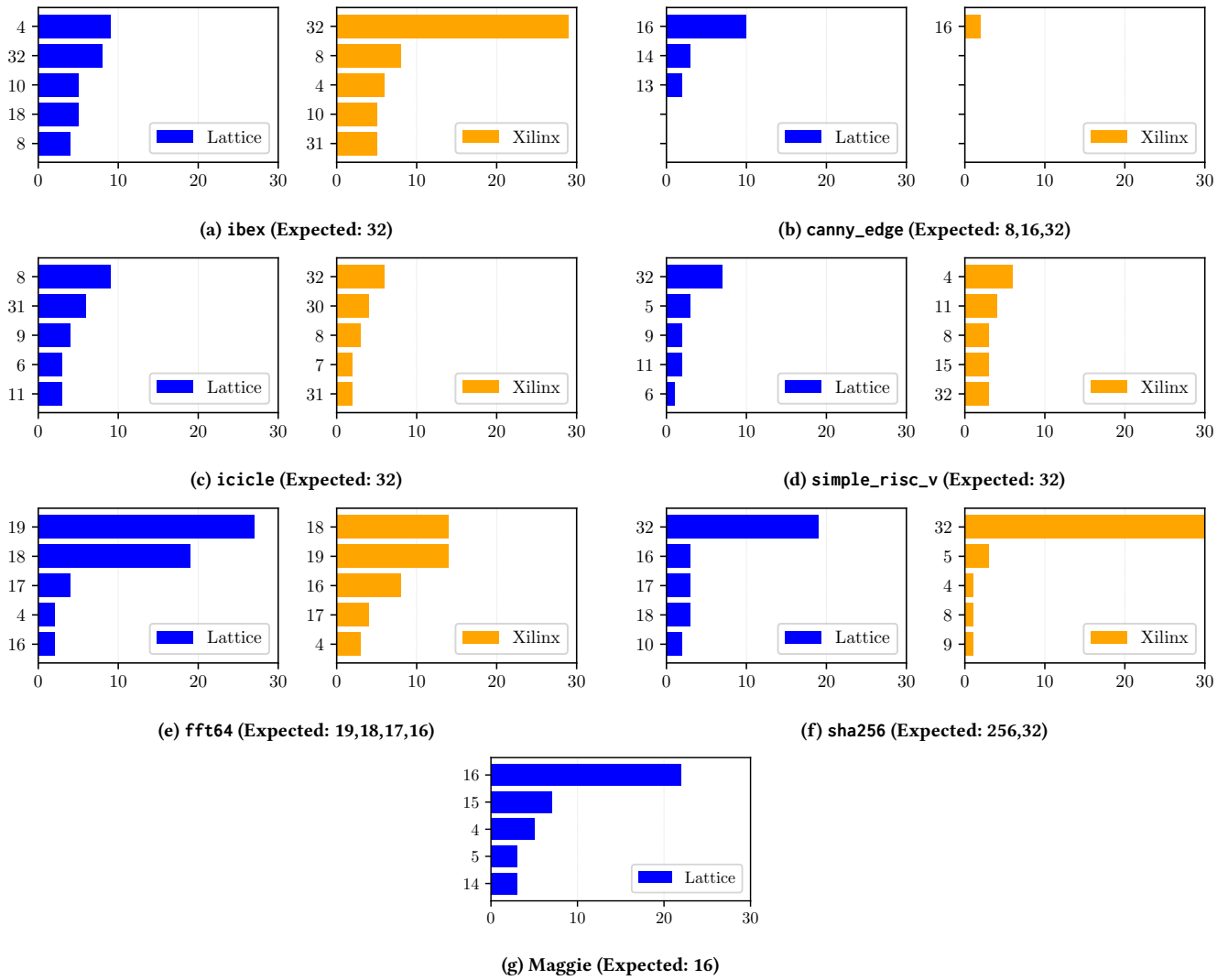


Figure 14: Evaluation of our word-level MUX detection using DANA.

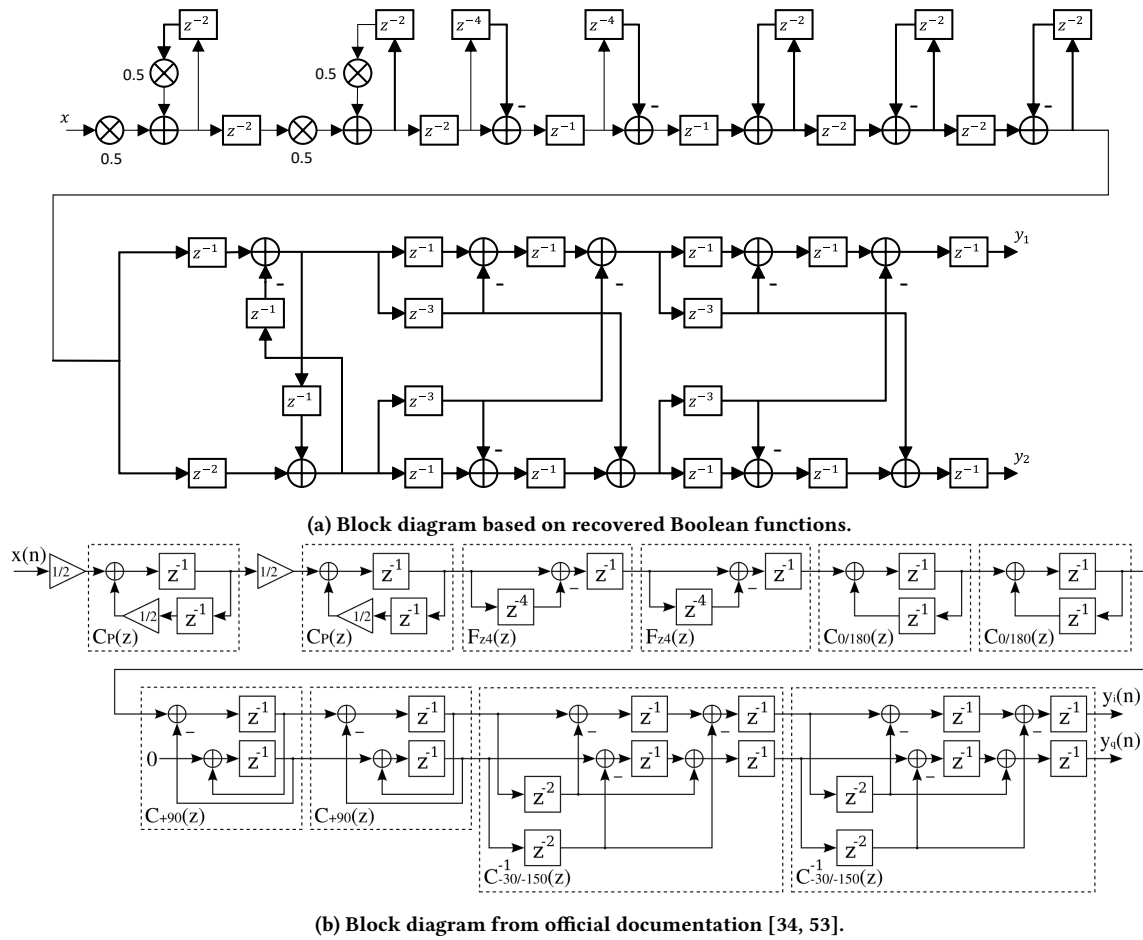


Figure 15: Comparison of Hilbert transformer block diagrams in the white-box case study.